

Absence of decoherence in the electron-wall system

Zilin Chen, Wayne Cheng-Wei Huang, and Herman Batelaan

Physics Department, University of Nebraska, Lincoln

(Dated: November 10, 2021)

Decoherence is associated with a dissipative environment as described by the Caldeira-Leggett equation. Anglin and Zurek predicted that a resistive surface could act as such a dissipative environment for a free electron wave passing close to it. We scrutinize Zurek's and other promising decoherence theoretical models by observing electrons passing by an optically excited GaAs surface and through a gold channel. The high resistivity of the GaAs surface and close proximity to the gold surface leads to strong decoherence within these decoherence models. In contradistinction, the observed contrast is high in our electron diffraction patterns. This implies lower decoherence rates than suggested by these models, making electron-matter-wave-guides and other technologies, where quantum coherence of electrons close to materials is important, a possibility.

Decoherence has been an important research area in the past few decades. It provides an explanation for the absence of macroscopic superposition and it may help to formulate a solution to the quantum measurement problem [1]. Quantum decoherence has been investigated in a number of physical systems. For example, one qubit can be decohered by interacting with an increasing number of other qubits that serve as a controllable environment [2]. Such a bottom-up approach moving to an ever increasing size of the environment can be complemented by a top-down approach where a quantum system interacts with a decreasingly complex mesoscopic environment. For example, a coherent molecular beam was decohered by a thermal bath. With lowered temperature, decoherence due to the bath was reduced [3]. In this example, a black-body photon gas serves as an environmental bath without local control parameters. The electron-wall system discussed in this paper may provide a locally-controllable decohering environment and serves as a testbed for decoherence theories. Moreover, both dissipation and decoherence can be measured for one system thus pointing to a test of quantum dissipation theory, i.e., the Caldeira-Leggett equation.

Theories specific for electron-wall interaction have been established based on different mechanisms. In 1997, Anglin, Paz, and Zurek [4] proposed environment-induced decoherence in the electron-wall system. As a free electron flies over the surface, dissipation due to Joule heating of the image charge in the wall occurs, which is linked to decoherence as in the well-known Caldeira-Leggett theory [5]. Theories by Scheel and Buhmann [6], Machnikowski [7], and Howie [8] also suggest the presence of environment-induced decoherence (but not based on dissipation). On the experimental side, observation of free electron decoherence was first claimed by Peter Sonnentag and Franz Hasselbach [9] in an experiment using an interferometer placed in close proximity to a silicon wall. The interference pattern contrast loss was identified to be a result of decoherence since the loss in contrast scales as a function of the distance between electrons and wall as Zurek's decoherence model predicts. However, the interaction with the wall was two orders of magnitude smaller than that predicted. Beierle

et al. [10] and Kerker et al. [11] followed up with similar experiments and confirmed the discrepancy. An alternative explanation for contrast loss is dephasing. While decoherence is time irreversible due to increased entropy, dephasing is reversible and can be caused by spurious effects such as patch potential. Chen et al. [12] modeled a general type of dephasing effect that caused contrast loss in an electron-wall system, suggesting that decoherence effects in previous experiments can actually be due to dephasing instead of decoherence. This may explain the inconsistency between experiments and current decoherence models. Therefore, an electron-wall system that exhibits unambiguously controllable decoherence in accordance with the Caldeira-Leggett theory for quantum dissipation is desirable.

In this paper, we test the experimental bounds of decoherence theories for the electron-wall system in two scenarios: (a) electrons passing over a GaAs wall where the resistivity is controlled by laser illumination, and (b) electrons passing through a gold channel. While Zurek's theory predicts a stronger decoherence rate in the GaAs experiment than that in Hasselbach's experiment, the observed diffraction pattern remains unaltered after electron interact with the wall. In the gold channel experiment, the electrons in close proximity to the surface were also expected to experience strong decoherence according to the decoherence theories, but again no contrast decrease was observed. We therefore conclude that no current theories are consistent with the absence of decoherence in our experiments.

We note that the amount of energy dissipation predicted was also not observed in our experiments. The absence of both dissipation and decoherence may imply that with improved resolution, electron-wall experiments may still provide a test for the Caldeira-Leggett theory.

In our setup, the electron beam is first collimated with two rectangular slits (Fig. 1(a)). The slits are separated by 24 cm. The width and height of the first and second slit are $13 \mu\text{m} \times 19 \mu\text{m}$ and $2 \mu\text{m} \times 10 \mu\text{m}$ respectively. The electron beam size is $3 \mu\text{m} \times 12 \mu\text{m}$ at the nanograting (whose periodicity is 100 nm), and its transverse coherence length is 400 nm. The electron beam density is low so that no electron-electron interaction is involved.

Paths that start from different slits interfere at the screen and produce individual diffraction peaks. The idea is that a surface brought close to these paths can cause decoherence between these paths and cause broadening of the diffraction peaks. This effect occurs at all diffraction peaks which serves as a consistency test. Therefore, the diffraction pattern is used to measure the decoherence rate in the experiment.

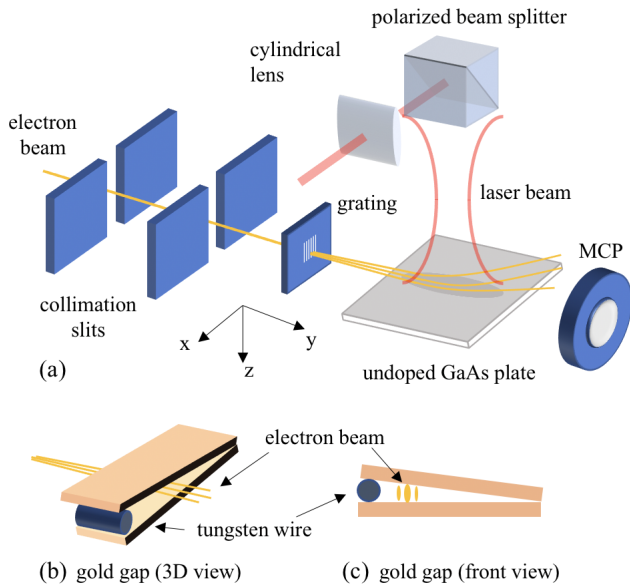


FIG. 1. Experimental setup. (a) The electron beam (yellow line) starts at the left top and travels to the bottom right. The first collimation slit is $12.7 \mu\text{m}$ wide and $19 \mu\text{m}$ tall. The second collimation slit, placed 25 cm downstream of the first collimation slit, is $2 \mu\text{m}$ wide and $10 \mu\text{m}$ tall. The grating periodicity is 100 nm with 50 nm slit widths. The diffracted electron beam passes $12 \mu\text{m}$ above the surface and intersects the laser beam. Laser induced charge carriers affect the electron diffraction pattern observed on the microchannel plate (MCP). The cylindrical lens is used to focus the beam on the GaAs surface. (b) For the gold gap experiment the GaAs plate is replaced by a gold gap. A tungsten wire is placed between two gold surfaces at one end to create the gap. The diameter of the tungsten wire is $15 \mu\text{m}$. The gold surface is 1.5 mm wide and 15 mm long. (c) A front view of the electron beam passing through the gold gap.

In the first experiment, the undoped GaAs plate ($1 \text{ cm} \times 1 \text{ cm}$) is placed $L = 3 \text{ mm}$ downstream after the grating with its surface parallel to the electron beam direction. The beam center is at a height of $12 \mu\text{m}$ corresponding to the surface. The electrons passing closest to the surface (at a height of $6 \mu\text{m}$) experience the strongest interaction and provide the most useful information for testing decoherence. The surface is illuminated with focused laser beam. The beam size is $150 \mu\text{m}$ perpendicular to the electron beam, and 1 cm parallel to the electron beam. The GaAs surface was illuminated with a 632 nm (super-bandgap) or a 1064 nm (sub-bandgap) laser for comparison. A charge distribution forms in the plate due to

the laser illumination and its field deflects the electron beam. The electron deflections are used to model the carrier behavior and obtain the resistivity which is given in Table. I. The details of the model are presented in the appendix. The resistivity is used as the input parameter in the decoherence models to calculate the decoherence rate and the energy dissipation rate. The second experiment involves the replacement of the GaAs surface with a gold gap (Fig. 1(a,b)) and will be described after the first experiment.

In Anglin and Zurek's original model [4], the Caldeira-Leggett master equation gives the evolution of the free electron's density matrix affected by the quantum Brownian motion. The equation shows that the resistivity influences the decoherence rate and the energy dissipation rate. It was stated that the model should work for resistivity in the range of 10^{-8} to $10^8 \Omega\text{cm}$ consistent with the experimental values. The decoherence time of the electron flying above a semiconductor wall is given by [4, 10],

$$\tau_{\text{dec}}^{\text{Zurek}} = \frac{4h^2}{\pi e^2 k_B T \rho} \frac{z^3}{(\Delta x)^2}, \quad (1)$$

where h is Planck's constant, k_B is Boltzmann's constant, $T = 300 \text{ K}$ is the temperature, ρ is the resistivity of the sample, z is the electron height above the surface, Δx is the path distance. Additionally, in our experiment, we should add two correction factors. The first factor is needed as the image charge patches under the electron path have overlap which reduces their capability to distinguish "which-way" information by a factor of $(z/\Delta x)^2$ [13]. The second factor is needed as the GaAs surface location is placed in the transition region between the near- and far-field of the electron diffraction. This means that paths from the slits to the detection do not separate entirely. Thus the overlap of two states reduces the environmental induced decoherence rate as compared to the rate for two well separated initial states (see Appendix D for details). The factor is $(\omega/\Delta x)^2$ where ω is the average width of a single slit beam above the surface.

We give numerical results from Zurek's model as well as other decoherence models (See appendix for details) in Table. I. In the table, Zurek's model predicts weak decoherence when GaAs is illuminated, while strong decoherence is expected without laser illumination. This is not observed in the diffraction pattern. The energy loss that accompanies the decoherence is computed to be so large for GaAs without illumination that the electron would lose most of its kinetic energy. This is not observed either and thus indicates that the method of calculating energy loss doesn't describe the physics for electron-semiconductors interaction.

To illustrate that we believe that our device is sensitive to changes in the number of decoherence events, $Rd = t_{\text{tof}}/\tau_{\text{dec}}^{\text{Zurek}}$, where t_{tof} is the time of flight, we plot the experimental data for an illuminated GaAs surface together with the simulated diffraction pattern for $Rd = 0.15$ and $Rd = 1$ (Fig. 2). The simulation and

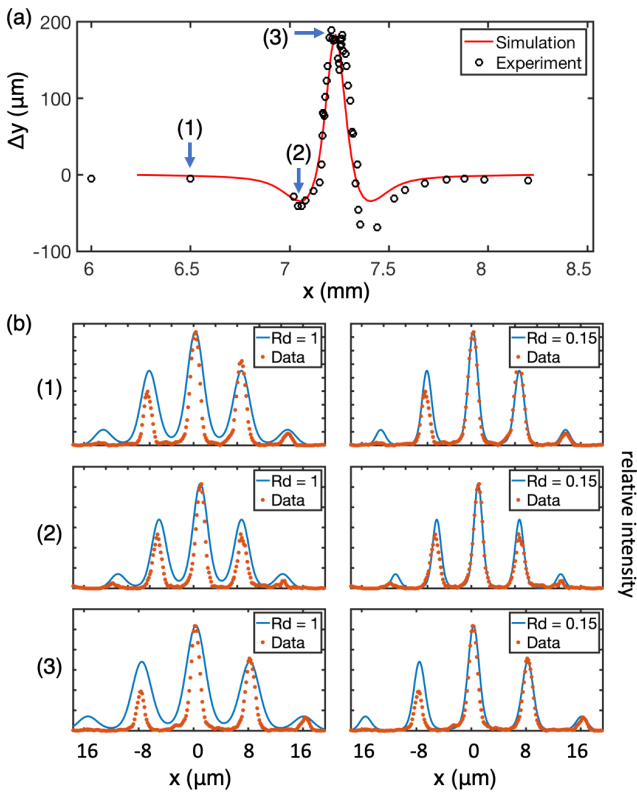


FIG. 2. Simulation and experiment. (a) The simulation (red solid line) is compared with the experimental data (open circles) for the vertical deflection of the electron beam as a function of the position of the electron beam. The laser is focussed at a position of approximately $x=7.25$ mm and has a waist of 0.15 mm. The laser-induced charging cause the deflection and changes the resistivity as a function of position by more than an order of magnitude. (b) At location (1), (2) and (3) the observed diffraction pattern is consistent with a weak loss of contrast (the decoherence amount is set to 0.15). A modest change of resistance accompanied by a change in the decoherence amount to 1 was not observed and supports the conclusion that decoherence does not play a role for electron-wall interaction in this experiment.

experiment agree for $Rd = 0.15$, but for $Rd = 1$ the simulated diffraction peaks are clearly wider than the experimental ones. For dark GaAs and the gold channel the decoherence amounts are so large that no simulated diffraction peaks (for Zurek's case) should be resolvable, while the experimental data show no change when the surface is brought towards the electron beam.

In the second experiment, we place a wedge-shaped gold gap at $L = 5$ mm from the grating with a gap size varying from $15 \mu\text{m}$ to $1 \mu\text{m}$. This gap is made of two separate pieces of gold-coated glass plates by clamping a tungsten wire on one end (Fig. 1(b) and 1(c)). The orientation of the wedge can be changed with respect to the incident direction of the electron beam (Fig. 3 (a,b)). When the tilt angle exceeds the geometric limit for unobstructed transmission, electrons reflect multiple times

with the gold surfaces of the gap. The average distance is very close considering multiple reflections. The predicted loss of energy and corresponding decoherence, both of a magnitude that is observable, are of interest for the purpose of confirming the Caldeira-Leggett equation. However, and surprisingly, no loss of contrast was observed (Fig. 3 (c)).

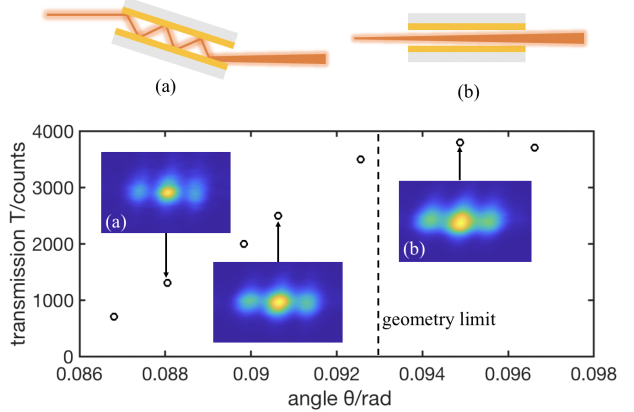


FIG. 3. Gold gap experiment. By changing the tilt angle of the gap, the transmission changes gradually. The circles in the figure shows the transmission rate in different tilt angle. The angle where the electron beam can straight pass is found with the maximum transmission rate. We present three diffraction patterns at different tilt angles. Diffraction pattern (a) corresponds to the beam having multiple reflections and the pattern (b) corresponds to the beam passing straight through the gap.

In our GaAs experiments, the electron is far away from the GaAs surface: $\Delta x/z < 1$ for our lateral coherence length of approximately 400 nm and the closest height of about 6 micron. This is taken into account in the correction factors. If we move the GaAs surface closer to the electron beam to decrease $\Delta x/z$ then the surface can accumulate charges due to secondary emissions [12] whose fields strongly distort the diffraction pattern. This overwhelms any potential decoherence signature in the electron diffraction pattern. Adding a second laser either continuously or chopped at a high rate can strongly reduce surface charges [15], which may provide a pathway to a controllable decohering environment for coherent electron beams.

In principle, there are several ways to identify decoherence. Auto-correlation imaging may assist in ruling out slow dephasing processes [16]. Holography can be used to directly measure coherence terms in the density matrix [17]. Agreement between experiment and model as a function of physical parameters may provide insight [18], and the simultaneous observation of energy dissipation and decoherence may establish the presence of decoherence, if the underlying entanglement follows the Caldeira-Leggett master equation [5]. The only model following that approach, Zurek's model, surprisingly does not provide an answer close to the experiment. This leaves the

TABLE I. The decoherence amount and energy loss are given for three models.

	GaAs (illuminated)	GaAs (dark)	Gold channel	Silicon ^a	Gold ^a
resistivity	$5\Omega m$	$2.5 \times 10^6 \Omega m$	$19 \times 10^{-8} \Omega m^b$	$1.5 \times 10^{-2} \Omega m$	$2.4 \times 10^{-8} \Omega m$
height	$6\mu m$	$6\mu m$	$0.85\mu m^c$	$1.7\mu m$	$1.7\mu m$
time of flight	$4.1 \times 10^{-10} s$	$4.1 \times 10^{-10} s$	$6.2 \times 10^{-11} s$	$4.1 \times 10^{-10} s$	$4.1 \times 10^{-10} s$
Zurek					
energy loss	18eV	$(9.0 \times 10^6 \text{ eV})$	48eV	2.4eV	$3.8 \times 10^{-6} \text{ eV}$
decoherence amount ^d	0.13	6.4×10^4	16	0.21	3.4×10^{-7}
Howie					
energy loss	0.19 eV	$4.7 \times 10^{-6} \text{ eV}$	$< 6 \times 10^{-4}$	0.18eV	$5.6 \times 10^{-4} \text{ eV}$
decoherence amount	1.49	1.5	0.25	5.8	0.32
Scheel-Markov					
decoherence amount	0.16	0.16	2.2	1.4(0.12)	0.0082

^a Using parameters of Beierle's experiment.

^b For a gold layer of 15 nm thickness. [14]

^c This is the maximum height as the electron collides with the surface. The gold gapsize is $1.7\mu m$.

^d The ratio Rd of time of flight over decoherence time. All values are calculated with corrections C1 and C2 (see appendix).

unexplained problem that the classical dissipation of electromagnetic waves is approximately correct [19], while the dissipation of the electromagnetic field of an electron traveling near a surface, or at least its feedback on the electron's motion, is not.

In the gold-gap experiment, the electrons are nominally very close to the material surface ($\Delta x/z > 1$), and still the decoherence rate is low. Our findings indicate that the search for electron-wall decoherence is currently at an interesting point. If decoherence rates are close to what can currently be probed by experiment, then it is likely that improved experimental techniques will provide a decoherence test-bed, and that improved modeling will provide insight. On the other hand, the observed rate is already small enough that it is likely that electron matter-optics can be confined to nearby material structures possibly leading to new technologies such as an "optical fiber" for electron waves. The transmission of an electron diffraction pattern through the gold gap supports this idea.

In terms of other decoherence models, Howie's model gave agreement with Hasselbach's experiment. In our experiments, some decoherence is predicted in both cases for GaAs experiment, and stronger decoherence for the earlier silicon experiment [10]. This was not observed in the previous or current experiment. The model developed by Scheel and Buhmann [6] didn't appear to be promising since no agreement was achieved until Kerker et. al [11] took out some approximations and reported an agreement with their experiments using a silicon wall. The same calculation for our experimental parameters, is consistent for the GaAs experiments, but the gold channel prediction is not in agreement with our observation.

In conclusion, all theoretical models to date fail to predict correct decoherence rates for existing experiments. Decoherence is smaller in practice than predicted. This

makes the search for an electron-wall testbed for theory harder. On the other hand, we found the diffraction pattern to remain unchanged as it passes through a gold gap with a large tilt angle. With such a tilt angle, the beam reflects multiple times. This may lead to electron-wave guide a possibility.

ACKNOWLEDGMENTS

We thank Prof. Zurek for suggesting the essential correction factor, Prof. Harry Ruda for advice on the effect of EL2 states, Prof. Scheel for pointing out the thermal correction factor, Prof. Stibor for pointing out the Karstens' thesis, and Prof. Liou for nano fabrication advice. The research was performed in part in the Nebraska Nanoscale Facility: National Nanotechnology Coordinated Infrastructure and the Nebraska Center for Materials and Nanoscience (and/or NERCF), which are supported by the National Science Foundation under Award ECCS: 2025298, and the Nebraska Research Initiative. The authors wish to thank Sai Mu and Jörg Malignretos for helpful discussions. We gratefully acknowledge support by the U.S. National Science Foundation under Grant No. PHY-1912504.

Appendix A: Three Theoretical models

In Zurek's theory, the relation between decoherence time and relaxation time is given by

$$\tau_{\text{dec}}^{\text{Zurek}} = \left(\frac{\lambda_{\text{th}}}{\Delta x} \right)^2 \tau_{\text{relax}}, \quad (\text{A1})$$

where Δx is the coherence length for our experiment and $\lambda_{\text{th}} = \hbar/\sqrt{mk_b T}$ is the thermal de Broglie wavelength of

the electron at room temperature (300 K). This equation, stemming from the Caldeira-Leggett master equation, describes the decoherence associated with energy loss when the electron passes above a resistive surface. The definition of relaxation time is $\tau_{\text{relax}} \equiv v / |\frac{dv}{dt}|$ according to Zeh [20]. The energy loss due to Ohmic dissipation used in Zurek's model comes from Boyer's theory [19]:

$$P = \frac{e^2 \rho v^2}{16 \pi z^3}. \quad (\text{A2})$$

By definition,

$$P = mv\dot{v} = \frac{mv^2}{\tau_{\text{relax}}} \rightarrow \tau_{\text{relax}} = \frac{mv^2}{P}, \quad (\text{A3})$$

in our experiment, the decoherence amount is calculated by

$$R_{\text{dec}}^{\text{Zurek}} = \int \frac{dt}{\tau_{\text{dec}}^{\text{Zurek}}} = \left(\frac{\Delta x}{\lambda_{\text{th}}} \right)^2 \frac{\Delta E}{mv^2}, \quad (\text{A4})$$

where ΔE is the energy loss during the interaction.

In Anglin and Zurek's original model [4], the Caldeira-Leggett master equation gives the evolution of the free electron's density matrix affected by the quantum Brownian motion. The model shows that the resistivity sets the decoherence rate and the energy dissipation rate. Anglin and Zurek state that the model should work for resistivity in the $10^{-8}\Omega \text{ cm}$ to $10^8\Omega \text{ cm}$ range. The decoherence time of the electron flying above the wall (semiconductor) is given by [4, 10],

$$\tau_{\text{dec}}^{\text{Zurek}} = \frac{4h^2}{\pi e^2 k_B T \rho} \frac{z^3}{(\Delta x)^2} / (C1 \times C2), \quad (\text{A5})$$

where h is Planck's constant, k_B is Boltzmann's constant, $T = 300 \text{ K}$ is the temperature, ρ is the resistivity of the sample, z is the electron height above the surface and Δx is the path distance. The path distance or equivalently the transverse coherence length Δx can be estimated using for the first slit a width of $12.7 \mu\text{m}$ and for the second slit a width of $2.0 \mu\text{m}$ and the distance between the slits, $D_s = 24 \text{ cm}$. The resulting angular divergence is multiplied with the electron's momentum to find the momentum uncertainty spread. From the uncertainty relation the position uncertainty spread can now be found and this equals the transverse coherence length, which is the maximum path distance and for which the decoherence time reaches its largest value. We used the resistivity of gold for a thin film (15 nm estimated from 5-7 minutes sputtering time) [14] as the channel substrate was sputtered with gold as opposed to the resistivity of bulk gold.

In our experiment, we should add two correction factors $C1$ and $C2$ (see Appendix D for details). The first factor is needed as the image charge patches under the electron path have overlap which reduces their capability to distinguish flying electron superposition states by a factor of $(z/\Delta x)^2$ [13]. The second factor follows the

same idea and is another overlap factor. It is needed as the GaAs surface location is placed in the transition region between the near- and far-field electron diffraction pattern. This means that the superposition of paths from the slits to the detection do not separate entirely. This correction shares the same idea that the overlap of two entangled states reduce the environmental induced decoherence rate compared to rate of two well separated initial states. It is estimated to be a factor of $(\omega/\Delta x)^2$ where ω is the average width of a single slit beam above the surface (Appendix C).

The model developed by Howie [8] is established in the electron microscopy community. In the model, decoherence is related to single excitation event probability e^{-P} of plasmons in the surface. In other words, if on average P events occur, the coherence is reduced by a factor e^{-P} . Howie's model gave agreement with Hasselbach's experiment. Some decoherence is predicted in both cases for the GaAs experiment, and stronger decoherence for the earlier silicon experiment [10]. The latter was not observed in the previous or current experiment (column 2 and 4 in Table 1 in the main text).

The general differential form of the single event probability P is

$$\frac{d^2 P(y, \omega, q_x)}{d\omega dq_x} = \frac{e^2 L}{2\pi^2 \varepsilon_0 \hbar v^2} \text{Im}\{\lambda_e\} \exp[-2\nu_0 z], \quad (\text{A6})$$

where λ_e is the retarded loss function,

$$\lambda_e = -\frac{2}{\nu + \nu_0 \varepsilon} + \frac{2\beta^2}{\nu + \nu_0}. \quad (\text{A7})$$

The parameters are defined by: $\beta = v/c$, $\nu_0^2 = [q_x^2 + (\omega/v)^2 - (\omega/c)^2]$, $\nu^2 = [q_x^2 + (\omega/v)^2 - \varepsilon(\omega)(\omega/c)^2]$. The dielectric function is given by $\varepsilon(\omega) \approx 1 + i\sigma(T)/\varepsilon_0 \omega m$, where σ is the conductivity of the surface. Previously, the event probability was given in different forms [8, 21]. First, Eq. (A6) is integrated over the plasmon frequency ω , and

$$P^{\text{Howie}} = \left(\frac{e^2 L \omega_m^2}{4\pi^2 \hbar \sigma v^2} \right) \int_{z/4\Delta x}^{\infty} \frac{\exp(-s)}{s} ds, \quad (\text{A8})$$

is obtained, where L is the path length which is the sample length, ω_m is the cut-off frequency for a semiconductor, and $\sigma = 1/\rho$ is the conductivity. A full transition from quantum to classical is predicted for parameters where $P \gg 1$. The upper bound of the plasmon frequency can be estimated from Eq. (A6) which falls off quickly so that above the upper bound it doesn't contribute to the integral [8, 10, 11]. To decohere, the flying electron must get a momentum recoil larger than its momentum spread and thus "sufficient to distinguish between the two interference paths" [8]. Relating this to our experiment this can be rephrased as follows. The transverse coherence length sets the momentum spread of the motional quantum state according to Heisenberg's

uncertainty principle. A momentum recoil larger than this momentum spread can thus distinguish the quantum state and cause decoherence. This implies that one should integrate the wave vector in the range of $q_x > \alpha\Delta x$, where α depends on the specific wavefunction and is of the order of one:

$$\int_{\alpha/\Delta x}^{\infty} \frac{\exp(-2zk_x)}{k_x} dk_x. \quad (\text{A9})$$

The value used in [8] here is 1/8 to get agreement with the experiment by Hasselbach [9] (note that there was a typographical error in [8]; α was mistakenly written as two [22]. The relative dielectric function, $\epsilon = 1 + i\sigma/\epsilon_0\omega$ given by the Drude model, is used in these papers. Not previously used for the calculation of decoherence rates, is that Eq. (A6) needs to be multiplied with the usual Boltzmann thermal correction factor $\coth(\frac{\hbar\omega}{2k_B T})$ [22, 23]. Note that even if Howie's model also predicts energy loss, it is not associated with the decoherence as an example of the Caldeira-Leggett equation. A newer version of this theory includes a thermal correction [23]

$$\frac{d^2 P(y, \omega, q_x)}{d\omega dq_x} = \coth(\hbar\omega/2k_B T) \frac{e^2 L}{2\pi^2 \epsilon_0 \hbar v^2} \text{Im}\{\lambda_e\} \exp[-2\nu_0 z] * C2, \quad (\text{A10})$$

Now the dielectric function $\epsilon(\omega)$ is given in reference [23, 24](eq 3.18 in [24]). The bounds on the ω integral are zero to the cut-off frequency. Howie uses $0.6 * 10^{12}$. For large cutoffs, the decoherence rate increases and the experimental test becomes stronger. The calculated decoherence amount should have affected the experimental diffraction significantly, but this is not observed.

The model developed by Scheel and Buhmann [6] also considers the image charge of the electron, but instead of using a classical approach to find the response [4, 19] a full quantum electrodynamics treatment is employed.

The interference visibility is given by $e^{-\Gamma[c]}$, where

$$\begin{aligned} \Gamma[c] = & -\frac{q^2 t}{\epsilon_0 \hbar (2\pi)^2} \int_{-\infty}^{\infty} \int_{-\infty}^{\infty} dk_x dk_y (1 - \cos(k_x L)) \\ & \times (2\bar{n}_{\text{th}}(|k_y v|) + 1) \times \frac{e^{-2k_{\parallel} z \gamma(k_x, k_y)}}{2k_{\parallel} \gamma(k_x, k_y)} \\ & \times \text{Im} \left(r_p(k_{\parallel}, |k_y v|) \gamma_v^2 + r_s(k_{\parallel}, |k_y v|) \frac{v^2 k_x^2}{c^2 k_{\parallel}^2} \right), \end{aligned} \quad (\text{A11})$$

where the reflection coefficients r_s and r_p depend on the resistivity, and

$$\bar{n}_{\text{th}}(\omega) = \left[e^{\hbar\omega/(k_B T)} - 1 \right]^{-1}. \quad (\text{A12})$$

is the Bose-Einstein distribution. Other parameters are defined as follows:

$$\gamma_v^2(\varphi) = 1 - \frac{v^2}{c^2} \cos^2 \varphi \quad (\text{A13})$$

and

$$\cos(\varphi) = k_y/k_{\parallel}, \quad (\text{A14})$$

where k_{\parallel} is the projection of the electron's wavevector in the x,y plane. These expressions were evaluated using some approximations. The theory didn't appear to be promising since no agreement with experiment was achieved until Kerker et. al [11] calculated (A8) numerically and report an agreement with their experiments using a silicon wall.

$$\begin{aligned} \epsilon(w) = & 1 - \frac{\omega_p^2}{\omega(\omega+i\gamma)} = \\ & 1 - \frac{\omega_p^2}{\omega^2 + \gamma^2} + i \frac{\omega_p^2 \gamma}{\omega(\omega^2 + \gamma^2)} = \epsilon_1 + i\epsilon_2 \end{aligned} \quad (\text{A15})$$

[25], where $r_s = \frac{\lambda - k}{\lambda + k}$ and $r_p = \frac{\epsilon(\omega)\lambda - k}{\epsilon(\omega)\lambda + k}$ are the reflectivities, and the parameters are defined by $\lambda = \left(K^2 - \frac{\omega^2}{c^2}\right)^{1/2}$, $k = \left(K^2 - \epsilon(\omega) \frac{\omega^2}{c^2}\right)^{1/2}$ and $K = k_{\parallel}$. The plasma frequency is given by $\omega_p = \sqrt{\frac{Ne^2}{\epsilon_0 m^*}}$, and the damping by $\gamma = \frac{Ne^2 \rho}{m^*}$. In the last equation the effective mass for GaAs electrons sub bandgap excitation or our "dark" case is given by [26]

$$m^* = m * 0.067, \quad (\text{A16})$$

while the effective mass for GaAs holes super bandgap excitation or our "illuminated" case is given by [26]

$$m^* = m * 0.34. \quad (\text{A17})$$

We repeated the same calculations for our experimental parameters, and find consistency for the GaAs experiment, but the gold channel prediction is not in agreement with our observation (column 3 bottom row in Table 1).

Appendix B: GaAs response modeling

In the GaAs experiment, since the electron beam width is much smaller than the laser focus width and thus the charge distribution, the lateral motion of the laser focus results in a measurement of the charge distribution on the GaAs surface. This charge distribution is used to model the carrier behavior. Super-bandgap and sub-bandgap illumination induce different charge distributions, and are recorded individually.

The surface charge due to the surface photovoltaic (SPV) effect has been calculated when the surface is uniformly illuminated [27]. For non-uniform illumination on the surface lateral electron transport can occur, which affects the magnitude of the SPV effect. In our experiment, the sample surface is illuminated in an oval shape which induces SPV gradients across the surface, leading to a non-uniform charge distribution. To explain the magnitude and shape of the charge distribution

for super-bandgap illumination, a rate equation model is used. The central elements in the model are the following. For 632 nm illumination, the photons can only penetrate for about $1/\alpha = 0.3 \mu\text{m}$ [28] into the surface. Electron and hole pairs are generated near the surface and start to diffuse. Electrons spread into the surroundings much faster than holes because the electron's diffusion coefficient typical value is $200 \text{ cm}^2/\text{s}$ compared to the hole's diffusion coefficient of $10 \text{ cm}^2/\text{s}$. Most generated electrons in the locally illuminated area are trapped by surface states. Consequently most holes, but only few electrons, escape. In this way, carriers form a charge distribution with a negative center and positive wings. The electric field created by the charge distribution prevents the holes from moving further away, and an equilibrium is reached (Fig. 4(a)). The sub-bandgap situation is described and modeled after the super-bandgap situation for comparison.

1. Super-bandgap model

In the super-bandgap model model, rate equations (called steady state continuity equations in [29]) are used to simulate diffusion, mobility, excitation, recombination and trapping:

$$\frac{dn(x)}{dt} = \frac{1}{e} \frac{dJ_n(x)}{dx} + G_n(x) - R_n(x), \quad (\text{B1})$$

$$\frac{dp(x)}{dt} = -\frac{1}{e} \frac{dJ_p(x)}{dx} + G_p(x) - R_p(x), \quad (\text{B2})$$

$$\frac{dn_t(x)}{dt} = G_t(x) - R_t(x), \quad (\text{B3})$$

where n , p and n_t are the negative, positive and trapped carrier densities, G and R are the generation and recombination rate, and e is the elementary charge magnitude. The current flows J_n and J_p are,

$$J_n(x) = e\mu_n n(x)\xi(x) + eD_n \frac{dn(x)}{dx}, \quad (\text{B4})$$

$$J_p(x) = e\mu_p p(x)\xi(x) - eD_p \frac{dp(x)}{dx}, \quad (\text{B5})$$

where ξ is electric field, $\mu_p = 300 \text{ cm}^2/\text{Vs}$, $\mu_n = 8000 \text{ cm}^2/\text{Vs}$ are typical mobilities, and $D_p = 10 \text{ cm}^2/\text{s}$, $D_n = 200 \text{ cm}^2/\text{s}$ are typical diffusion coefficients for positive and negative carriers. In Eq. (B1), the total thermal recombination rate R_n consists of the capture rate into

the valence band, $r_{n \rightarrow p}^{th}$, and the capture rate into the trapping states $r_{n \rightarrow t}^{th}$,

$$R_n = r_{n \rightarrow p}^{th} + r_{n \rightarrow t}^{th} \quad (\text{B6a})$$

$$r_{n \rightarrow p}^{th} = c_{n \rightarrow p}^{th} np \quad (\text{B6b})$$

$$r_{n \rightarrow t}^{th} = c_{n \rightarrow t}^{th} np_t, \quad (\text{B6c})$$

where the thermal recombination rate is proportional to both the positive (p) and negative (n) carrier density, and the proportionality constants (for capture driven by thermal recombination) are given by $c_{n \rightarrow p}^{th}$ and $c_{n \rightarrow t}^{th}$. Generation term for the conduction band G_n are composed of the thermal generation term $g_{p \rightarrow n}^{th}$ and the optical generation term $g_{p \rightarrow n}^{opt}$ which depicts electron excitation from valence band to conduction band; and the thermal generation term $g_{t \rightarrow n}^{th}$ and optical generation term $g_{t \rightarrow n}^{opt}$ describes excitation from the trapping states to the conduction band,

$$G_n = g_{p \rightarrow n}^{th} + g_{p \rightarrow n}^{opt} + g_{t \rightarrow n}^{th} + g_{t \rightarrow n}^{opt} \quad (\text{B7a})$$

$$g_{p \rightarrow n}^{th} = c_{n \rightarrow p}^{th} n_0 p_0 \quad (\text{B7b})$$

$$g_{p \rightarrow n}^{opt} = F(1 - R)\eta e^{-(x - x_0)^2/\omega^2} \quad (\text{B7c})$$

$$g_{t \rightarrow n}^{th} = e_{t \rightarrow n} n_t \quad (\text{B7d})$$

$$g_{t \rightarrow n}^{opt} = \sigma_{t \rightarrow n}^{opt} F n_t, \quad (\text{B7e})$$

where n_0 and p_0 are the intrinsic carrier densities (about 10^6 cm^{-3}) without illumination, F is the photon flux ($\approx 10^{18} \text{ cm}^{-2} \text{s}^{-1}$), $R = 0.3$ is reflectivity [30], $\eta = 0.7$ is the quantum efficiency [31], x_0 is the beam center location and ω is the beam width. The thermal excitation rates and optical excitation rate to the trapping states are, $e_{t \rightarrow n}$ and $\sigma_{t \rightarrow n}^{opt}$, respectively. And in the Eq. (B2) and Eq. (B3) the equalities

$$G_p = G_n \quad (\text{B8a})$$

$$G_t = r_{n \rightarrow t}^{th} \quad (\text{B8b})$$

$$R_p = r_{n \rightarrow p}^{th} \quad (\text{B8c})$$

$$R_t = g_{t \rightarrow n}^{th} + g_{t \rightarrow n}^{opt} \quad (\text{B8d})$$

$$(\text{B8e})$$

hold.

In addition to modeling the carrier dynamics, we use a semi-classical electron trajectory simulation to model the deflection of the beam. The electron diffraction is described by the usual quantum mechanical distribution, while the electron motion above the GaAs plate is obtained by numerically solving Newton's equation. The electric field used in the equation of motion is obtained by summing Coulomb's law over the charge distribution given by the carrier dynamics model. Details for this method can be found in our previous work [12]. We found that the beam shift in the vertical direction is proportional to the total charge integrated over the surface directly below the beam path. This means that the curvature of the electron trajectories is negligible for the

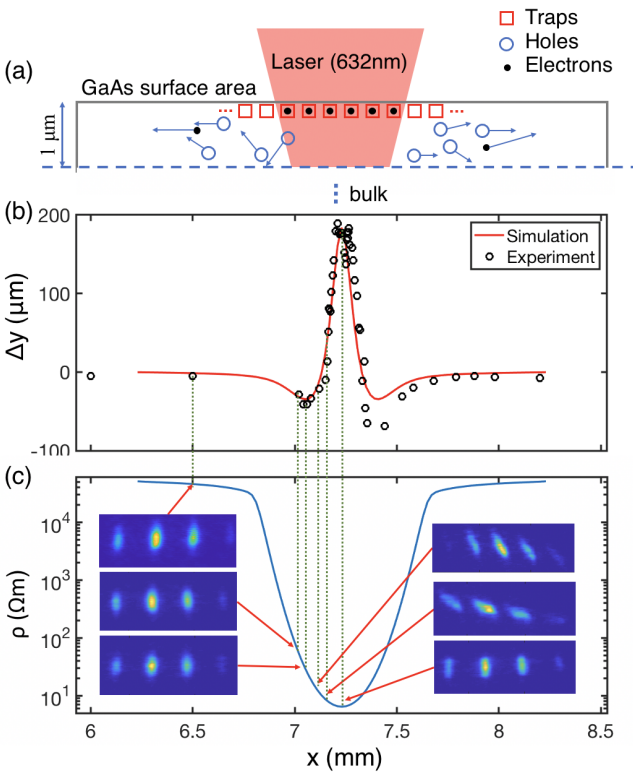


FIG. 4. Super-bandgap excitation. (a) A schematic picture of super-bandgap illumination is shown. Laser light (632 nm) penetrates to a depth of about 0.3 micron at the GaAs sample surface, and excites electrons from the valence band to the conduction band. After excitation, electrons and holes start to diffuse, and most electrons are trapped in surface states. (b) The laser beam is scanned laterally (x -axis) and the electron beam deflection (black circles) is measured. In the center area, the deflection is away from the surface. The result of a charge carrier model (red solid line) is shown. (c) The inferred resistivity (blue solid line) shows several orders of magnitude variation. The electron diffraction patterns exhibit varying degrees of rotation but the contrast of the diffraction pattern does not change.

experimental parameters. It also suggests that the vertical deflection is a good measurement for the longitudinal (y -axis) integrated charge distribution.

No integration over the charge distribution in the z -direction is done. This is motivated by the small laser penetration depth as compared to the height above the surface. The carrier dynamics are thus simplified to one dimension (x). The electron beam deflection was observed while the laser focus was scanned laterally (x). The charge distribution is then obtained from the combination of the mathematical model and the trajectory simulation (Fig. 4(b)). The experimental data matches the model well. The experimentally higher side wing on the right can be caused by non uniformities in the laser beam. The diffraction pattern show no broadening (Fig. 4(c)) and the rotations of the diffraction orders is due to local field gradients.

The temporal behavior is another clue for the existence of trapping states. To investigate the temporal response, the deflection was measured while the laser was chopped (Fig. 5) to reveal charging effects in timescales of 0.1–1 s. In GaAs, SPV is usually formed in microseconds [15, 29], but that is without the presence of trapping states. The charge distribution recovery time is also slow and exceeds one second (Fig. 5). This confirms earlier observations [15]. We now describe the details of the laser chopping experiment. The electron beam position is recorded with our camera. When the laser is turned off, the electron beam starts at a location defined as the zero. Now the chopper is rotating and the laser is turned on. The electron beam position moves up further with light pulse when the chopper is in the open position. The beam position does not fully recover when the chopper is in the closed position at a chopping frequency of 4–20 Hz. This implies a charging time slower than 1/4 s. When reaching a semi-steady state, the beam oscillates between two locations whose distance is smaller than the deflection from the zero location. These two beam locations are the corresponding chop-close (blue circular dots) and chop-open (red triangular dots) deflection data for each chopping frequency (Fig. 5). The simulation (solid lines) agrees fairly well with the experiment.

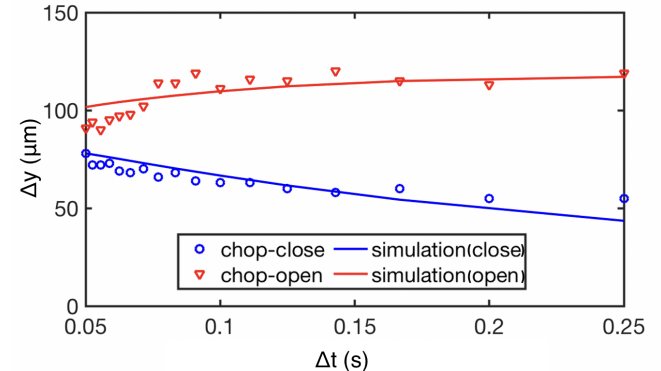


FIG. 5. Temporal dependence of deflection. The data shown was taken at the center peak location (see Fig. 4) with the laser chopped continuously at a range of frequencies. The chop-opening time Δt , corresponds to the chopping frequency (the laser on and off times are equal). Deflection zero is defined as the deflection without any laser present.

2. Sub-bandgap model

In the sub-bandgap model, photons are much less strongly absorbed than for the super-bandgap situation and can penetrate deeply into the bulk [28]. Even if the photon energy is less than the bandgap energy, electrons are still pumped to the conduction band due to defect-assisted excitation [32]. Electrons and holes generated at different depths diffuse into the bulk. Surface states trapping is not the leading effect anymore, and it is not

included in the model for simplicity. A simple sketch illustrates the main elements of the model (Fig. 6(a)). The detection beam is about 12 microns away from the surface, while the bulk distribution extends throughout the 300 microns thick GaAs plate. The charges near the surface make the dominant contribution to the deflection of the free electrons. The deflection shows large side wings and a relatively small center peak across the sample (Fig. 6(b)) indicating that the surface has a net negative charge and more electrons are accumulated near the surface. Given that charges are generated throughout the bulk and a non-zero-sum charge distribution resides at the surface, the dimension perpendicular to the surface must be included in the model. Therefore, the continuity equations are extended to two dimensions,

$$\frac{dn(x, y)}{dt} = \frac{1}{e} \vec{\nabla}_{x, y} \cdot \vec{J}_n(x, y) + G_n(x) - R_n(x), \quad (B9)$$

$$\frac{dp(x, y)}{dt} = -\frac{1}{e} \vec{\nabla}_{x, y} \cdot \vec{J}_p(x, y) + G_p(x) - R_p(x), \quad (B10)$$

where,

$$\vec{J}_n(x, y) = e\mu_n n(x, y) \vec{\xi}(x, y) + eD_n \vec{\nabla}_{x, y} n(x, y), \quad (B11)$$

$$\vec{J}_p(x, y) = e\mu_p p(x, y) \vec{\xi}(x, y) - eD_p \vec{\nabla}_{x, y} p(x, y), \quad (B12)$$

Comparing with the equations for super-bandgap excitations, generation and recombination only have the terms $r_{n \rightarrow p}^{th}$, $g_{p \rightarrow n}^{th}$, and $g_{p \rightarrow n}^{opt}$; there are no trapping terms. Because of the internal scattering and reflection, the laser width deep in the bulk in the model is bigger than that given by free propagation. The sub-bandgap laser is composed of two Gaussians beams whose widths are about 150 μm and 750 μm , where the wider Gaussian beam is five times weaker. When calculating the detection beam trajectories, charges near the surface within 10 μm are used. Positive and negative charges in deep layers tend to cancel each other's field close to the surface. If there would have been uniform charge component from the charge distribution in the deeper layers, then one could expect an electric field with a long range above the surface. This can be ruled out experimentally by moving the probing electron beam to a distance of 100 micron above the surface. At this distance there is no discernible deflection. The experimental deflection data agrees well with the simulation (Fig. 6(b)). The experimental diffraction data again shows no appreciable broadening of the diffraction peaks (Fig. 6(c)).

The assumptions in the simple model can be investigated further to represent to complex nature of the surface more accurately. For example, the laser can heat the surface to create a temperature gradient in the material. This might form an internal electric field referred to as the Peltier-Seebeck effect [33]. However, in the experiment, the laser intensity is only 2 mW, and such a

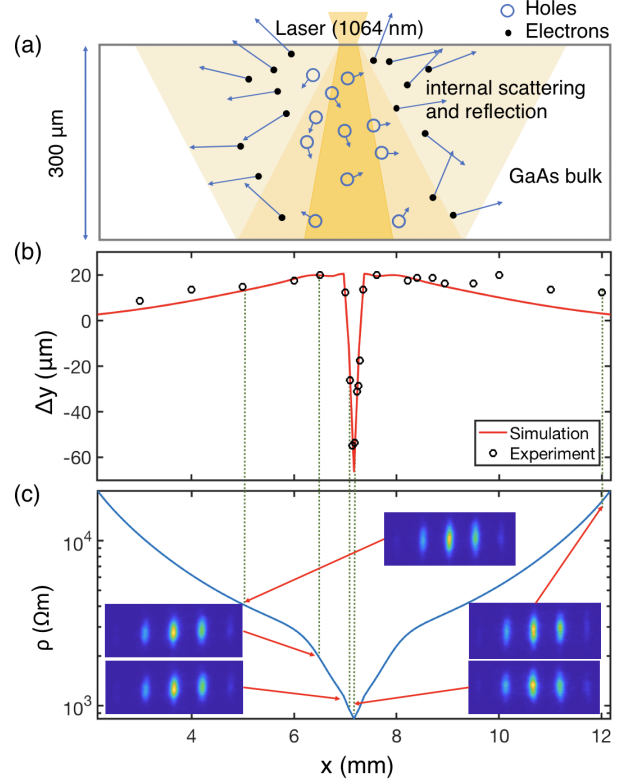


FIG. 6. Sub band-gap excitation. (a) A schematic picture of sub-bandgap illumination in the bulk is shown. Laser light (1064 nm) can penetrate deeply into the GaAs bulk. Electrons and holes can diffuse freely in the bulk. The detection electron beam above the surface is sensitive to charges near the surface because the bulk thickness is 30 times larger than the distance between detection beam and the surface. (b) The laser beam is scanned laterally (x -axis) and the electron beam deflection (black circles) is measured. In the center area, the deflection is towards the surface. The result of a charge carrier model (red solid line) is shown. (c) The inferred resistivity (blue solid line) is shown. Several electron diffraction MCP images exhibit little distortion as compared to super-bandgap excitation because of smaller induced surface charge (weaker fields). Charge is distributed throughout the whole sample, while in the super-bandgap situation, the charges distribute only in limited area.

low intensity laser cannot create a significant temperature gradient in a time duration of about one second. The fitting parameters are consistent with previous experimental data. For example, in the sub-band gap situation, defect-assisted excitation is assumed in the model. EL2 defects are one of the well known defects with a high density [34].

Appendix C: Correction factors

To calculate the decoherence rate it is assumed in the theoretical models that the surface states induced by the electron-surface interaction are non-overlapping. To il-

TABLE II. Decoherence rate correction factors. C1 and C2 are used with Zurek's model, while C2 is used for Howie's and Scheel's model.

	GaAs	Gold channel	Silicon/Gold ^a
decoherence correction	$C1, C2 = 0.0044, 0.1$	$C1, C2 = 1, 0.18$	$C1, C2 = 0.055, 0.1$

^a Using parameters of Beierle's experiment.

lustrate this, consider two slits separated by Δx on the left and right (Fig. 7). The surface states, $|s_L\rangle$, and $|s_R\rangle$ (indicated by red disks), that are induced by the electron paths $|L\rangle$ and $|R\rangle$, can provide complete which-way information on the electron when they are non-overlapping. Tracing, for example, the resulting entangled state $|L, s_L\rangle + |R, s_R\rangle$ over the surface states completely removes the electron path coherence. However, when the surface states are partially overlapping, the which-way information is not completely removed by tracing. The magnitude of this effect is given by $|\langle s_L | s_R \rangle|^2$. For an electron at a height h above the surface, and a Coulombic interaction potential that scales with $1/r$, the approximate size s of the image charge patch is estimated by h itself. As $w \sim \Delta x$, the correction factor applied to the decoherence rate is $C1 = \sim (\Delta x/h)^2$, as suggested by Zurek [13]. When Δx exceeds h the correction factors equals one. An additional correction factor needs to be applied. When the electron paths are in the near-field the paths are completely distinguishable. However, in the transition from near- to far-field they are not. To illustrate this, instead of considering the paths, it is useful to consider single slit diffraction from the two slits considered (Fig. 7, blue shade triangles). This is estimated by propagating a Gaussian beam to the middle of the surface. The width at that location is given

by $w = w_0 \sqrt{1 + (L\lambda_{dB}/\pi w_0)^2}$. The overlap between the two diffracted beams is approximated by the second correction factor $C2 = ((\Delta x/w)^2$ for $\Delta x < w$. Both correction factors reduce the decoherence rate. The divergence angle of the single slit diffraction pattern is given by $\theta = \Delta p_y/p \sim \Delta y_s/\hbar p$, where Δy_s is the slit width and p the electron's momentum. The transition to the far-field regime occurs when $L\theta \sim \Delta y_s/2$.

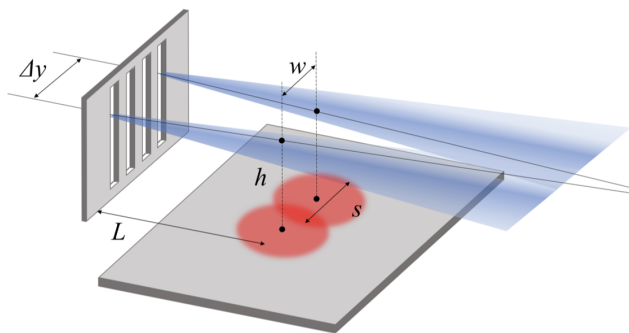


FIG. 7. Correction factors. A symbolic picture of diffraction from a grating. The image charge patches (red disks) are located underneath the electron positions (black dots). The electron positions are located on paths (black lines). Diffraction from single slits is indicated by blue cones to illustrate the transition from the near- to far-field. As the image charge patch overlap increases, or the single slit diffraction cones overlap increases, which-way information is reduced and the decoherence rate slows by a correction factor (see text).

[1] W. H. Zurek, Rev. Mod. Phys. **75**, 715 (2003).

[2] T. Brydges, A. Elben, P. Jurcevic, B. Vermersch, C. Maier, B. P. Lanyon, P. Zoller, R. Blatt, and C. F. Roos, Science **364**, 260 (2019).

[3] L. Hackermüller, K. Hornberger, B. Brezger, A. Zeilinger, and M. Arndt, Nature **427**, 711 (2004).

[4] J. R. Anglin, J. P. Paz, and W. H. Zurek, Phys. Rev. A **55**, 4041 (1997).

[5] W. H. Zurek, in *Frontiers of Nonequilibrium Statistical Physics* (Springer, 1986) pp. 145–149.

[6] S. Scheel and S. Y. Buhmann, Phys. Rev. A **85**, 030101 (2012).

[7] P. Machnikowski, Phys. Rev. B **73**, 155109 (2006).

[8] A. Howie, Ultramicroscopy **111**, 761 (2011).

[9] P. Sonnentag and F. Hasselbach, Phys. Rev. Lett. **98**, 200402 (2007).

[10] P. J. Beierle, L. Zhang, and H. Batelaan, New J. Phys. **20**, 113030 (2018).

[11] N. Kerker, R. Röpke, L. M. Steinert, A. Pooch, and A. Stibor, New J. Phys. **22**, 063039 (2020).

[12] Z. Chen and H. Batelaan, Europhys. Lett. **129**, 40004 (2020).

[13] W. H. Zurek, (private communication).

[14] T. Gilani and D. Rabchuk, Can. J. Phys. **96**, 272 (2018).

[15] P. E. J. Lagowski and A. Morawski, Semicond. Sci. Technol. **7**, A211 (1992).

[16] Z. Chen, P. Beierle, and H. Batelaan, Phys. Rev. A **97**, 043608 (2018).

[17] A. Tonomura, Rev. Mod. Phys. **59**, 639 (1987).

[18] B. Barwick, G. Grönninger, L. Yuan, S.-H. Liou, and H. Batelaan, J. Appl. Phys. **100**, 074322 (2006).

[19] T. H. Boyer, Physical Review A **9**, 68 (1974).

[20] E. Joos, H. D. Zeh, C. Kiefer, D. J. Giulini, J. Kupsch, and I.-O. Stamatescu, *Decoherence and the appearance of a classical world in quantum theory* (Springer Science & Business Media, 2013).

[21] F. Forstmann, A. Gras-Marti, T. Ferrell, R. Warmack, and K. Mamola, Physical Review B **44**, 4884 (1991).

[22] A. Howie, (private communication).

[23] A. Howie, Ultramicroscopy **203**, 52 (2019).

[24] K. Karstens, *Pfaddekhärenz von Elektronen und Ionen in der Nähe dielektrischer Oberflächen*, Master's thesis, University of Rostock, Germany (2014).

[25] E. D. Palik, *Handbook of optical constants of solids*, Vol. 3 (Academic press, 1998).

[26] B. Van Zeghbroeck, Colarado University **34** (2004).

[27] L. Kronik and Y. Shapira, Surf. Sci. Rep. **37**, 1 (1999).

[28] M. D. Sturge, Phys. Rev. **127**, 768 (1962).

[29] Q. Liu, C. Chen, and H. Ruda, J. Appl. Phys. **74**, 7492 (1993).

[30] H. R. Philipp and H. Ehrenreich, Phys. Rev. **129**, 1550 (1963).

[31] V. R. M. Milanova, A. Mintairov and K. Smekalin, J. Electron. Mater. **28**, 35 (1999).

[32] G. M. Martin, Appl. Phys. Lett. **39**, 747 (1981).

[33] H. Goldsmid, J. Electron. Mater. **40**, 1254 (2011).

[34] K. Germanova and C. Hardalov, Appl. Phys. A **43**, 117 (1987).